

# Interface Between Topological and Superconducting Qubits

Liang Jiang,<sup>1</sup> Charles L. Kane,<sup>2</sup> John Preskill<sup>1</sup>

<sup>1</sup> *Institute for Quantum Information, California Institute of Technology, Pasadena, CA 91125, USA and*  
<sup>2</sup> *Department of Physics and Astronomy, University of Pennsylvania, Philadelphia, Pennsylvania 19104, USA*  
 (Dated: October 30, 2018)

We propose and analyze an interface between a topological qubit and a superconducting flux qubit. In our scheme, the interaction between Majorana fermions in a topological insulator is coherently controlled by a superconducting phase that depends on the quantum state of the flux qubit. A controlled phase gate, achieved by pulsing this interaction on and off, can transfer quantum information between the topological qubit and the superconducting qubit.

*Introduction* Topologically ordered systems are intrinsically robust against local sources of decoherence, and therefore hold promise for quantum information processing. There have been many intriguing proposals for topological qubits, using spin lattice systems [1], p+ip superconductors [2], and fractional quantum Hall states with filling factor 5/2 [3]. The recently discovered topological insulators [4] can also support topologically protected qubits [5]. Meanwhile, conventional systems for quantum information processing (*e.g.*, ions, spins, photon polarizations, superconducting qubits) are steadily progressing; recent developments include high fidelity operations using ions [6] and superconducting qubits [7], long-distance entanglement generation using single photons [8, 9], and extremely long coherence times using nuclear spins [10].

Interfaces between topological and conventional quantum systems have also been considered recently [11, 12]. Hybrid systems [13, 14] may allow us to combine the advantages of conventional qubits (high fidelity readout, universal gates, distributed quantum communication and computation) with those of topological qubits (robust quantum storage, protected gates). In this paper, we propose and analyze an interface between a topological qubit based on Majorana fermions (MFs) at the surface of a topological insulator (TI) [5] and a conventional superconducting (SC) flux qubit based on a Josephson junction device [15]. The flux qubit has two basis states, for which the SC phase of a particular SC island has two possible values. In our scheme, this SC phase coherently controls the interaction between two MFs on the surface of the TI. This coupling between the MFs and the flux qubit provides a coherent interface between a topological and conventional quantum system, enabling exchange of quantum information between the two systems.

*Topological Qubit* The topological qubit can be encoded with four Majorana fermion operators  $\{\gamma_i\}_{i=1,2,3,4}$ , which satisfy the Majorana property  $\gamma_i^\dagger = \gamma_i$  and fermionic anti-commutation relation  $\{\gamma_i, \gamma_j\} = \delta_{ij}$ . A Dirac fermion operator can be constructed from a pair of MFs  $\Gamma_{ij}^\dagger = (\gamma_i - i\gamma_j)/\sqrt{2}$ , defining a two dimensional Hilbert space labeled by  $n_{ij} = \Gamma_{ij}^\dagger \Gamma_{ij} = 0, 1$ . The two basis states for the topological qubit, each with an even number of Dirac fermions, are  $|0\rangle_{\text{topo}} = |012034\rangle$  and

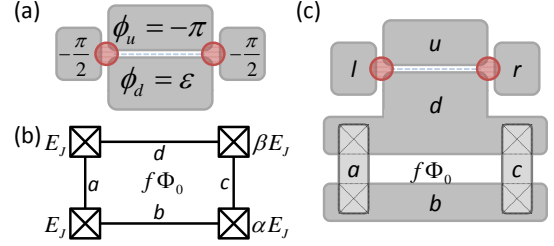


FIG. 1: (color online). On the surface of TI, patterned SC islands can form (a) STIS quantum wire, (b) flux qubit, and (c) hybrid system of topological and flux qubits. (a) Two MFs (red dots) are localized at two SC tri-junctions, connected by an STIS quantum wire (dashed blue line). The coupling between the MFs is controlled by the SC phases  $\phi_d = \epsilon$  and  $\phi_u = -\pi$ . (b) A flux qubit consists of four JJs connecting four SC islands ( $a, b, c, d$ ) in series, enclosing an external magnetic flux  $f\Phi_0$ . (c) The hybrid system consists of an STIS wire and a flux qubit. The STIS wire (between islands  $d$  and  $u$ ) couples the MFs, with coupling strength controlled by the flux qubit. The SC phase  $\phi_c$  can be tuned by a phase-controller (not shown), and  $\phi_d = \phi_c \pm \theta_4^*$  with the choice of  $\pm$  sign depending on the state of the flux qubit.

$$|1\rangle_{\text{topo}} = |112134\rangle.$$

The MFs can be created on the surface of a TI patterned with s-wave superconductors [5]. Due to the proximity effect [16], Cooper pairs can tunnel into the TI; hence the effective Hamiltonian describing the surface includes a pairing term, which has the form  $V = \Delta_0 e^{i\phi} \psi_\uparrow^\dagger \psi_\downarrow^\dagger + h.c.$  (where  $\psi_\uparrow^\dagger, \psi_\downarrow^\dagger$  are electron operators), assuming that the chemical potential is close to the Dirac point [17]. Here  $\phi$  is the SC phase of the island. Each MF is localized at an SC vortex that is created by an SC tri-junction (*i.e.*, three separated SC islands meeting at a point, see Fig. 1(a)). The MFs can interact via a superconductor-TI-superconductor (STIS) wire (Fig. 1(a)) that separates the SC islands  $d$  and  $u$  with  $\phi_d = \epsilon$  and  $\phi_u = -\pi$ , respectively. For a narrow STIS wire with width  $W \ll v_F/\Delta_0$ , the effective Hamiltonian is

$$H^{\text{STIS}} = -iv_F \tau^x \partial_x + \delta_\epsilon \tau^z, \quad (1)$$

where  $v_F$  is the effective fermi velocity,  $\delta_\epsilon = \Delta_0 \cos(\phi_d - \phi_u)/2 = -\Delta_0 \sin \epsilon/2$ , and  $\tau^{x,z}$  are Pauli

matrices acting on the wire's two zero energy modes [5]. As shown in Fig. 1(a), the STIS wire connects two localized MFs (indicated by two red dots at the tri-junctions) separated by distance  $L$ ; these are two of the four MFs comprising the topological qubit. The coupling between the MFs (denoted as  $\gamma_1$  and  $\gamma_2$ ) via the STIS wire can be characterized by the Hamiltonian  $\tilde{H}_{12}^{\text{MF}} = iE(\varepsilon)\gamma_1\gamma_2/2$ , with an induced energy splitting  $E(\varepsilon)$  depending on the SC phase  $\varepsilon$ . The effective Hamiltonian for the topological qubit is

$$H_{12}^{\text{MF}} = -\frac{E(\varepsilon)}{2}\mathbf{Z}_{\text{topo}}. \quad (2)$$

where  $Z_{\text{topo}} = (|0\rangle\langle 0| - |1\rangle\langle 1|)_{\text{topo}}$ .

In Fig. 2(a), we plot  $E(\varepsilon)$  as a function of a dimensionless parameter  $\Lambda_\varepsilon \equiv \frac{\Delta_0 L}{v_F} \sin \frac{\varepsilon}{2}$ . For  $\Lambda_\varepsilon \gg 1$  and  $0 < \varepsilon < \pi/2$  [5], the energy splitting  $E(\varepsilon) \approx 2|\delta_\varepsilon|e^{-\Lambda_\varepsilon} \sim 0$  is negligibly small for localized MFs at the end of the wire, as the wavefunctions are proportional to  $e^{-\Lambda_\varepsilon x/L}$  and  $e^{-\Lambda_\varepsilon(L-x)/L}$ . On the other hand, for  $\Lambda_\varepsilon \lesssim 1$ , the two MFs are delocalized and  $E(\varepsilon)$  becomes sensitive to  $\varepsilon$ . We emphasize that  $E(\varepsilon)$  is a non-linear function of  $\varepsilon$  [18], which enables us to switch the coupling on and off.

*Flux Qubit* The SC island  $d$  can also be part of an SC flux qubit (Fig. 1(b)), with  $\phi_d = \varepsilon = \varepsilon^0$  or  $\varepsilon^1$  depending on whether the state of the flux qubit is  $|0\rangle_{\text{flux}}$  or  $|1\rangle_{\text{flux}}$  as shown in Fig. 2(b,c). Therefore, the Hamiltonian  $H_{12}^{\text{MF}}$  couples the flux qubit and the topological qubit. Assuming a small *phase separation*  $\Delta\varepsilon \equiv \varepsilon^0 - \varepsilon^1 \ll \pi/2$ , we can switch off the coupling  $H_{12}^{\text{MF}}$  by tuning  $\varepsilon^{0,1}$  to satisfy  $v_F/L\Delta_0 \ll \varepsilon^{0,1} < \pi/2$  [5], so that the MFs are localized and uncoupled with negligible energy splitting  $E(\varepsilon^0) \approx E(\varepsilon^1) \sim 0$ . We can also switch on the coupling  $H_{12}^{\text{MF}}$  by adiabatically ramping to the parameter regime  $\varepsilon^{0,1} \lesssim v_F/L\Delta_0$  to induce a nonnegligible  $|E(\varepsilon^0) - E(\varepsilon^1)| \sim \Delta_0\Delta\varepsilon$ . Because flux qubit designs with three Josephson junctions (JJs) [15, 19] are not amenable to achieving a small phase separation  $\Delta\varepsilon \ll \pi/2$  (Appendix), we are motivated to modify the design of the flux qubit by adding more JJs.

As shown in Fig. 1(b), our proposed flux qubit consists of a loop of four Josephson junctions in series that encloses an applied magnetic flux  $f\Phi_0$  ( $f \approx 1/2$  and  $\Phi_0 = h/2e$  is the SC flux quantum). The Hamiltonian for the flux qubit is

$$H^{\text{flux}} = T + U, \quad (3)$$

with Josephson potential energy  $U = \sum_{i=1,2,3,4} E_{J,i}(1 - \cos \theta_i)$ , and capacitive charging energy  $T = \frac{1}{2} \sum_{i=1,2,3,4} C_i V_i^2$ . For the  $i$ -th JJ,  $E_{J,i}$  is the Josephson coupling energy,  $\theta_i$  is the gauge-invariant phase difference,  $C_i$  is the capacitance, and  $V_i$  is the voltage across the junction [15, 19]. In addition, there are relations satisfied by the phase accumulation around the loop  $\sum_i \theta_i + 2f\pi \equiv 0 \pmod{2\pi}$  and the voltage across each junction  $V_i = \left(\frac{\Phi_0}{2\pi}\right) \dot{\theta}_i$  [16]. The parameters are chosen as follows: the first two JJs have equal

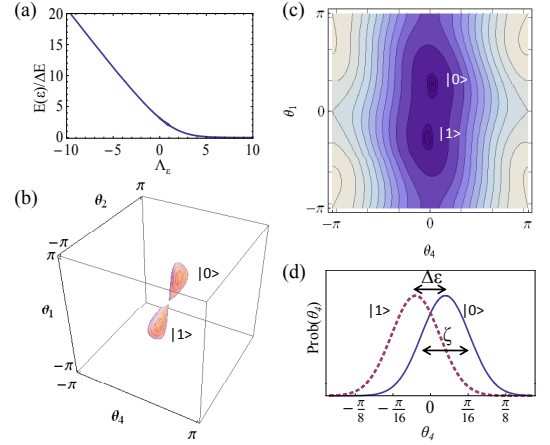


FIG. 2: (color online). (a) The energy splitting  $E(\varepsilon)$  (in units of  $\Delta E = v_F/L$ ) as a function of  $\Lambda_\varepsilon = \frac{\Delta_0 L}{v_F} \sin \varepsilon/2$ . (b) A contour plot of potential energy  $U$  as a function of  $\{\theta_1, \theta_2, \theta_4\}$  with  $\theta_3 = \pi - \theta_1 - \theta_2 - \theta_4$ . There are two potential minima associated with flux qubit states  $|0\rangle$  and  $|1\rangle$ . (c) A contour plot of  $U$  as a function of  $\{\theta_1, \theta_4\}$  with  $\theta_1 = \theta_2$  and  $\theta_3 = \pi - 2\theta_1 - \theta_4$ . (d) Marginal probability distributions of  $\theta_4$  associated with states  $|0\rangle$  (blue solid line) and  $|1\rangle$  (red dashed line). The parameters are  $E_J/EC = 80$  and  $\{E_{J,i}/E_J\}_{i=1,2,3,4} = \{1, 1, \alpha = 0.8, \beta = 10\}$ .

Josephson coupling energy  $E_{J,1} = E_{J,2} = E_J$ , the third JJ has  $E_{J,3} = \alpha E_J$  with  $0.5 < \alpha < 1$ , and the fourth JJ has  $E_{J,4} = \beta E_J$  with  $\beta \gg 1$ . For JJs with the same thickness but different junction area  $\{A_i\}$ ,  $E_{J,i} \propto A_i$  and  $C_i \propto A_i$ . The charging energies can be defined as  $EC_{,1} = EC_{,2} = EC = \frac{e^2}{2C_1}$ ,  $EC_{,3} = \alpha^{-1}EC$  and  $EC_{,4} = \beta^{-1}EC$ . For these parameters and  $f \approx 1/2$ , the system has two stable states with persistent circulating current of opposite sign. We identify the flux qubit basis states with the two potential minima  $|0\rangle_{\text{flux}} = |\{\theta_i^*\}\rangle$  and  $|1\rangle_{\text{flux}} = |\{-\theta_i^*\}\rangle$  (modulo  $2\pi$ ), as illustrated in Fig. 2(b,c).

When  $\beta \rightarrow \infty$ , we may neglect the fourth junction and this system reduces to the previous flux qubit design with three JJs [15, 19]. For  $\beta \gg 1$ , there is a small phase difference across the fourth JJ (Appendix),  $\theta_4 = \pm\theta_4^* \approx \pm \frac{\sqrt{4\alpha^2 - 1}}{2\alpha} \frac{1}{\beta}$ , where the choice of  $\pm$  sign depends on the direction of the circulating current. We may write  $\theta_4 = \mathbf{Z}_{\text{flux}}\theta_4^*$ , with  $\mathbf{Z}_{\text{flux}} = (|0\rangle\langle 0| - |1\rangle\langle 1|)_{\text{flux}}$ . The fourth JJ connects SC islands  $c$  and  $d$ , and if we fix  $\phi_c$  relative to  $\phi_u$  with a phase-controller [26], then  $\phi_d$  will be  $\varepsilon^0 = \phi_c + \theta_4^*$  or  $\varepsilon^1 = \phi_c - \theta_4^*$  depending on the state of the flux qubit. The separation

$$\Delta\varepsilon \approx \frac{\sqrt{4\alpha^2 - 1}}{\alpha} \frac{1}{\beta} \quad (4)$$

between the two possible values of  $\phi_d$  becomes small, as we desired, when  $\beta$  is large.

Aside from this small phase separation, there are also *quantum fluctuations* in  $\theta_4$  due to the finite capacitance.

Near its minimum at  $\pm\{\theta_i^*\}$ , the potential energy is approximately quadratic; therefore, for  $\beta \gg 1$ , the dynamics of  $\theta_4$  can be well described by a harmonic oscillator (HO) Hamiltonian

$$H^{\text{HO}} = \frac{p_{\theta_4}^2}{2M_4} + \frac{E_{J,4}}{2} (\theta_4 - \mathbf{Z}_{\text{flux}}\theta_4^*)^2, \quad (5)$$

where the effective mass is  $M_4 = \frac{1}{8E_{C,4}}$  and the canonical momentum  $p_{\theta_4}$  satisfies  $[\theta_4, p_{\theta_4}] = i$  (with  $\hbar \equiv 1$ ). We may rewrite  $H^{\text{HO}} = (a^\dagger a + 1/2)\omega$  and  $\theta_4 = \mathbf{Z}_{\text{flux}}\theta_4^* + \zeta(a^\dagger + a)/\sqrt{2}$ , where the oscillator frequency is  $\omega = \sqrt{8E_J E_C}$  and the magnitude of quantum fluctuations is  $\zeta = \left(\frac{8E_C}{E_J}\right)^{1/4} \beta^{-1/2}$ . Fig. 2(d) shows the probability distribution functions  $p_{0/1}(\theta_4) \approx \frac{1}{\zeta\sqrt{\pi}} e^{-(\theta_4 \mp \theta_4^*)^2/\zeta^2}$  associated with  $|0\rangle_f$  and  $|1\rangle_f$ . The magnitude of the quantum fluctuations  $\zeta$  is comparable to the phase separation  $\Delta\varepsilon$ ; indeed  $\zeta \propto \beta^{-1/2}$  may even dominate the phase separation  $\Delta\varepsilon \propto \beta^{-1}$  for large  $\beta$  (Fig. 3). [27] Therefore, we should consider both the phase separation and the quantum fluctuations.

*Hybrid System* The Hamiltonian for the hybrid system of topological and flux qubits (Fig. 1(c)) is:

$$H = H^{\text{HO}} + H_{12}^{\text{MF}} = (a^\dagger a + 1/2)\omega - \frac{1}{2}E(\varepsilon)\mathbf{Z}_{\text{topo}} \quad (6)$$

where  $\varepsilon = \phi_c + \theta_4 = \phi_c + \mathbf{Z}_{\text{flux}}\theta_4^* + \zeta(a^\dagger + a)/\sqrt{2}$ . In both flux qubit basis states, the oscillator is in its ground state with  $\langle a^\dagger a \rangle = 0$ . To first order in the small parameter  $\delta \equiv \left. \frac{\zeta}{\omega} \frac{dE(\phi)}{d\phi} \right|_{\phi=\phi_c} \ll 1$ , the Hamiltonian becomes

$$H = H^{\text{HO}} - \frac{1}{2}(\langle E_0 \rangle |0\rangle\langle 0| + \langle E_1 \rangle |1\rangle\langle 1|)_{\text{flux}} \otimes \mathbf{Z}_{\text{topo}} + O(\delta^2)$$

where  $\langle E_{0/1} \rangle \equiv \int d\theta_4 E(\phi_c + \theta_4) p_{0/1}(\theta_4)$ .

Up to a single-qubit rotation, the effective Hamiltonian coupling the flux and topological qubits is

$$H_I = \frac{g}{4} \mathbf{Z}_{\text{flux}} \mathbf{Z}_{\text{topo}} \quad (7)$$

with coupling strength  $g = \frac{\langle E_1 \rangle - \langle E_0 \rangle}{(E(\varepsilon^1) - E(\varepsilon^0)) + \frac{1}{4}(E''(\varepsilon^1) - E''(\varepsilon^0))\zeta^2} \approx O(\zeta^3)$ . The first term arises from the phase separation and the second term from the quantum fluctuations; corrections higher order in  $\zeta \ll 1$  are small.

Because the energy splitting function  $E(\varepsilon)$  is highly non-linear, we may tune  $\phi_c$  to  $\phi_{\text{off}}$  such that  $v_F/L\Delta_0 \ll \varepsilon^{0,1} = \phi_{\text{off}} \pm \Delta\varepsilon/2 < \pi/2$  and switch off the coupling  $g \approx \Delta_0 \Delta\varepsilon e^{-|\phi_{\text{off}}| \Delta_0 L/2v_F} \sim 0$ . On the other hand, we may adiabatically ramp  $\phi_c$  to  $\phi_{\text{on}} \lesssim v_F/L\Delta_0$ , which effectively switches on the coupling  $g \approx \Delta_0 \Delta\varepsilon$ . By adiabatically changing  $\phi_c$  from  $\phi_{\text{off}} \rightarrow \phi_{\text{on}} \rightarrow \phi_{\text{off}}$  with  $\int g(t) dt = \pi$ , we can implement the controlled-phase ( $\text{CP}_{t,f}$ ) gate between the topological ( $t$ ) and flux ( $f$ ) qubits. With Hadamard gates  $\text{Had}_f$ , we can achieve

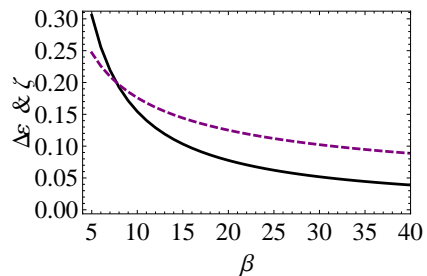


FIG. 3: (color online). Comparison between the phase separation  $\Delta\varepsilon \propto \beta^{-1}$  (dark solid line) and the magnitude of quantum fluctuations  $\zeta \propto \beta^{-1/2}$  (purple dashed line), assuming  $E_J/E_C = 80$ .

$\text{CNOT}_{t,f} = \text{Had}_f \cdot \text{CP}_{t,f} \cdot \text{Had}_f$ , which flips the flux qubit conditioned on  $|1\rangle_t$  and can be used for quantum non-demolition measurement of the topological qubit [11, 20]. Furthermore, with Hadamard gates  $\text{Had}_t$  (implemented by exchanging two MFs [3, 5]), we can achieve the swap operation  $\text{SWAP}_{t,f} = (\text{Had}_t \cdot \text{Had}_f \cdot \text{CP}_{t,f})^3$ . Finally, with  $\text{CP}_{t,f}$ ,  $\text{Had}_t$  and single-qubit rotations  $U_f$ , we can achieve arbitrary unitary transformations for the two-qubit hybrid system of flux and topological qubits [13, 14].

*Imperfections* There are four relevant imperfections for the coupled system of flux and topological qubits [28]. The first imperfection is related to the tunneling between  $|0\rangle_{\text{flux}}$  and  $|1\rangle_{\text{flux}}$  of the flux qubit, with tunneling rate  $t \sim \omega \exp(-\sqrt{E_J/E_C})$ . The coupling between flux and topological qubits should be strong enough,  $g \gg t$ , to suppress the undesired tunneling probability  $\eta_{\text{tunnel}} \approx (t/g)^2$ .

The next imperfection comes from undesired excitations of the oscillators. According to the Hamiltonian  $H$  for the hybrid system, the oscillators may be excited via interaction  $E(\phi_c + \theta_4) = E(\phi_c + \mathbf{Z}_{\text{flux}}\theta_4^*) + \frac{dE}{d\varepsilon} \zeta \frac{\hat{a}_1^\dagger + \hat{a}_1}{\sqrt{2}} + \dots$ . The excitation probability can be estimated as  $\eta_{\text{excite}} \approx \left(\frac{\zeta}{2\omega} \frac{dE}{d\varepsilon}\right)^2$ . Since  $|\frac{dE}{d\varepsilon}| \lesssim \Delta_0$ ,  $\zeta \approx \left(\frac{8E_C}{E_J}\right)^{1/4} \beta^{-1/2}$ , and  $\omega = \sqrt{8E_J E_C}$ , we estimate  $\eta_{\text{excite}} \lesssim \frac{1}{20\beta} \left(\frac{\Delta_0}{E_J}\right)^2 \sqrt{\frac{E_J}{E_C}}$ .

The third imperfection is due to the finite length of the STIS wire, which limits the fidelity for the topological qubit itself. When we switch off the coupling between the flux and topological qubits by having  $\phi_c = \phi_{\text{off}}$  and  $\Lambda_{\phi_{\text{off}}} \gg 1$  for the STIS wire, there is an exponentially small energy splitting  $E \sim \Delta_0 e^{-\Lambda_{\phi_{\text{off}}}}$ .

The last relevant imperfection is associated with the excitation modes of the quantum wire, with excitation energy  $E' \approx v_F/L$  [5]. Occupation of these modes can potentially modify the phase separation of the flux qubit. Therefore, we need sufficiently low temperature to exponentially suppress the occupation of these modes by the

factor  $e^{-E'/k_B T}$ .

*Physical Parameters* We may choose the following design parameters for the flux qubit:  $\alpha = 0.8$ ,  $\beta = 10$ ,  $E_J/E_C = 80$ , and  $E_J = 200 (2\pi)$  GHz. Both phase separation and quantum fluctuations depend sensitively on  $\beta$  (see Fig. 3), with  $\Delta\varepsilon \approx 0.16$  and  $\zeta \approx 0.18$ . Meanwhile, the flux qubit has plasma oscillation frequency  $\omega \approx 60 (2\pi)$  GHz, energy barrier  $\Delta U \approx 0.26 E_J$ , tunneling rate  $t \approx 1.8 \sqrt{E_J E_C} \exp[-0.7 (E_J/E_C)^{1/2}] \approx 70 (2\pi)$  MHz; these parameters only marginally depend on  $\beta$  (Appendix).

For mesoscopic aluminum junctions with critical current density 500 A/cm<sup>2</sup>, the largest junction ( $E_{J,A} = \beta E_J$ ) has an area of about 1  $\mu\text{m}^2$  [15]. For the topological qubit, it is feasible to achieve the parameters  $\Delta_0 \sim 0.1\text{meV} \approx 25 (2\pi)\text{GHz}$ ,  $v_F \sim 10^5\text{m/s}$ ,  $L \sim 5\mu\text{m}$ , and  $T = 20\text{mK}$ . For the interface, the effective coupling is  $g \sim \Delta_0 \Delta\varepsilon \sim 2 (2\pi)\text{GHz}$ . Therefore, we have imperfections  $\eta_{\text{tunnel}} \sim 10^{-3}$ ,  $\eta_{\text{excite}} \lesssim 10^{-3}$ ,  $e^{-\Lambda_{\phi_{\text{off}}}} \approx e^{-20|\sin \phi_{\text{off}}/2|} < 10^{-3}$  (assuming  $\phi_{\text{off}} \approx \pi/4$ ), and  $e^{-E'/k_B T} < 10^{-3}$  [29].

*Phase Qubit* A similar interface can be constructed to couple the SC phase qubit [7, 21] and the topological qubit. A phase qubit is just a JJ with a fixed DC-current source  $I$ . The phase qubit Hamiltonian is  $H^{\text{phase}} = T + U^{\text{phase}}$ , where  $T = \frac{1}{2} E_C V^2$  and  $U^{\text{phase}} = -I \Phi_0 \phi - I_0 \Phi_0 \cos \phi$ . The qubit can be encoded in the two lowest energy states,  $|0\rangle_{\text{phase}}$  and  $|1\rangle_{\text{phase}}$ , with magnitude of quantum fluctuations  $\zeta_0$  and  $\zeta_1$ , respectively. The coupling strength between phase and topological qubits can be estimated as  $g^{\text{phase}} \approx E''(\varepsilon) (\zeta_1^2 - \zeta_0^2)$ .

*Notes added* It was recently proposed to use the Aharonov-Casher (AC) effect for quantum non-

demolition measurement of a topological qubit [11, 12]. This proposal, which applies in the parameter regime  $\alpha > 1$  where the flux qubit has two possible tunneling pathways, exploits the observation that whether two tunneling paths interfere destructively or constructively can be controlled by the state of the topological qubit. In contrast, our proposal, which applies in the parameter regime  $\alpha < 1$  where the flux qubit has only one tunneling pathway, exploits the non-linearity of the energy splitting  $E(\varepsilon)$  to achieve a controlled-phase coupling between the topological and flux qubits. Recently, the related work [22] appeared.

*Conclusion* We have proposed and analyzed a feasible interface between flux and topological qubits. Our proposal uses a flux qubit design with four JJs, such that the two basis states of the qubit have a small phase separation  $\Delta\varepsilon$  on a particular superconducting island, enabling us to adiabatically switch on and off the coupling between the flux and topological qubits. Such interfaces may enable us to store and retrieve quantum information using the topological qubit, to repetitively readout the topological qubit with a conventional qubit, or to switch between conventional and topological systems for various quantum information processing tasks.

We are especially indebted to Mikhail Lukin for inspiring discussions. We also thank Anton Akhmerov, Jason Alicea, Erez Berg, David DiVincenzo, Garry Goldstein, Netanel Lindner and Gil Refael for helpful comments. This work was supported by the Sherman Fairchild Foundation, by NSF grants DMR-0906175 and PHY-0803371, by DOE grant DE-FG03-92-ER40701, and by NSA/ARO grant W911NF-09-1-0442.

- 
- [1] A. Y. Kitaev, *Annals of Physics* **303**, 2 (2003).  
[2] N. Read and D. Green, *Phys. Rev. B* **61**, 10267 (2000).  
[3] C. Nayak, S. H. Simon, A. Stern, M. Freedman, and S. Das Sarma, *Rev. Mod. Phys.* **80**, 1083 (2008).  
[4] M. Z. Hasan and C. L. Kane, *Rev. Mod. Phys.* **82**, 3045 (2010).  
[5] L. Fu and C. L. Kane, *Phys. Rev. Lett.* **100**, 096407 (2008).  
[6] R. Blatt and D. Wineland, *Nature (London)* **453**, 1008 (2008).  
[7] J. Clarke and F. K. Wilhelm, *Nature (London)* **453**, 1031 (2008).  
[8] D. L. Moehring, P. Maunz, S. Olmschenk, K. C. Younge, D. N. Matsukevich, L. M. Duan, and C. Monroe, *Nature (London)* **449**, 68 (2007).  
[9] E. Togan, Y. Chu, A. S. Trifonov, L. Jiang, J. Maze, L. Childress, M. V. G. Dutt, A. S. Sorensen, P. R. Hemmer, A. S. Zibrov, et al., *Nature (London)* **466**, 730 (2010).  
[10] M. V. G. Dutt, L. Childress, L. Jiang, E. Togan, J. Maze, F. Jelezko, A. S. Zibrov, P. R. Hemmer, and M. D. Lukin, *Science* **316**, 1312 (2007).  
[11] F. Hassler, A. R. Akhmerov, C.-Y. Hou, and C. W. J. Beenakker, *New J. Phys.* **12**, 125002 (2010).  
[12] J. D. Sau, S. Tewari, and S. Das Sarma, *Phys. Rev. A* **82**, 052322 (2010).  
[13] L. Jiang, G. K. Brennen, A. Gorshkov, K. Hammerer, M. Hafezi, E. Demler, M. D. Lukin, and P. Zoller, *Nat. Phys.* **4**, 482 (2008).  
[14] M. Aguado, G. K. Brennen, F. Verstraete, and J. I. Cirac, *Phys. Rev. Lett.* **101**, 260501 (2008).  
[15] J. E. Mooij, T. P. Orlando, L. Levitov, L. Tian, C. H. van der Wal, and S. Lloyd, *Science* **285**, 1036 (1999).  
[16] M. Tinkham, *Introduction to superconductivity* (McGraw Hill, New York, 1996), 2nd ed.  
[17] T. D. Stanescu, J. D. Sau, R. M. Lutchyn, and S. Das Sarma, *Phys. Rev. B* **81**, 241310 (2010).  
[18] L. Jiang, C. L. Kane, and J. Preskill, arXiv: **1010.5862** (2011).  
[19] T. P. Orlando, J. E. Mooij, L. Tian, C. H. van der Wal, L. S. Levitov, S. Lloyd, and J. J. Mazo, *Phys. Rev. B* **60**, 15398 (1999).  
[20] J. D. Sau, R. M. Lutchyn, S. Tewari, and S. Das Sarma, *Phys. Rev. Lett.* **104**, 040502 (2010).  
[21] J. M. Martinis, S. Nam, J. Aumentado, and C. Urbina, *Phys. Rev. Lett.* **89**, 117901 (2002).

- [22] P. Bonderson and R. M. Lutchyn, Phys. Rev. Lett. **106**, 130505 (2010).
- [23] I. Chiorescu, Y. Nakamura, C. J. P. M. Harmans, and J. E. Mooij, Science **299**, 1869 (2003).
- [24] P. Bertet, I. Chiorescu, G. Burkard, K. Semba, C. J. P. M. Harmans, D. P. DiVincenzo, and J. E. Mooij, Phys. Rev. Lett. **95**, 257002 (2005).
- [25] J. R. Friedman, V. Patel, W. Chen, S. K. Tolpygo, and J. E. Lukens, Nature (London) **406**, 43 (2000).
- [26] An SC phase-controller can fix the phase difference between two SC islands. It can be implemented by controlling either the external flux or the current (Appendix).
- [27] Despite the large quantum fluctuations in  $\theta_4$  ( $\zeta > \Delta\varepsilon$ ), the two quantum states of the flux qubit are well localized because the two potential minima are widely separated in the  $\theta_1$  direction (see Fig. 2(c)).
- [28] We assume that flux qubit parameters can be accurately measured, and hence ignore fabrication uncertainties.
- [29] The SQUID circuit that measures the flux qubit is another potential source of error, as it may introduce an additional plasma mode with low frequency  $\omega'$ . Assuming  $\omega' \sim 2(2\pi)\text{GHz}$  [23]), we may choose  $g = 200(2\pi)\text{MHz}$  and  $t = 10(2\pi)\text{MHz}$ , so that  $\omega' \gg g \gg t \gg 1/T_2$ . If the flux qubit's spin-echo coherence time  $T_2$  is long ( $\approx 4\mu\text{s}$  [24]), a 1% error rate can be achieved.

### Appendix A: Flux Qubits

We describe our design of the SC flux qubit that prepares an SC island with SC phase  $\varepsilon = \varepsilon^0$  or  $\varepsilon^1$  depending on the flux qubit state  $|0\rangle_{\text{flux}}$  or  $|1\rangle_{\text{flux}}$ . The phase of the SC island can coherently control the coupling between the two Majorana fermions at the end of the STIS wire. We would like to have a small phase separation  $\Delta\varepsilon \equiv \varepsilon^1 - \varepsilon^0 \ll \pi/2$ , so that we can easily switch off the coupling  $H_{12}^{\text{MF}}$  when we do not want to couple the Majorana fermions (MFs).

The previous design of flux qubit with three JJs [15, 19], however, is not amenable to achieving a small phase separation  $\Delta\varepsilon \ll \pi/2$ , because of the following reason. The three JJs have Josephson energy  $E_{J,1} = E_{J,2} = E_J$  and  $E_{J,3} = \alpha E_J$  [15, 19]. The phase difference across the first junction is  $\theta = \pm \cos^{-1} \frac{1}{2\alpha}$ . By choosing  $\alpha = \eta + 1/2$  and  $\eta \ll 1$ , there is a small phase separation  $\Delta\varepsilon = 2|\theta| \approx 4\eta^{1/2}$ . However, the energy barrier for the tunneling is significantly suppressed  $\Delta U = 2\alpha - (2 - \frac{1}{2\alpha}) E_J \approx 4\eta^2 E_J \sim \theta^4 E_J$ . The action associated with the tunneling is  $S \approx \theta \sqrt{\Delta U/E_C} \approx \theta^3 \sqrt{E_J/E_C} \propto \theta^3 E_J$ , where the last step uses the property that  $E_C \propto 1/E_J$ . In order to maintain a similar tunneling matrix element between the two potential minima, it requires the unfavorable scaling  $E_J \propto 1/\theta^3$ . For example, to achieve  $\theta = 0.1$ , we have to increase the area of the Josephson junction by  $\sim 10^3$ . Practically, it would also be very challenging to have a precise value of  $\alpha = \frac{1}{2} + \frac{\theta^2}{4} = 0.5025$ , which fine tunes the phase separation  $\Delta\varepsilon$ . In contrast, the four-junction design of flux qubit has a favorable scaling of  $E_{J,4} = \beta E_J \propto 1/\theta$  and there is no fine-tuned parameter. This motivates us to

redesign the flux qubit with more Josephson junctions.

As shown in Fig. 4, the flux qubit consists of a loop of four JJs in series that encloses an external magnetic flux  $f\Phi_0$  ( $f \approx 1/2$  and  $\Phi_0 = h/2e$  is the SC flux quantum). The first two JJs have equal Josephson coupling energy  $E_{J,1} = E_{J,2} = E_J$ ; the third JJ has coupling energy  $E_{J,3} = \alpha E_J$ , with  $0.5 < \alpha < 1$ ; the coupling in the fourth JJ is  $E_{J,4} = \beta E_J$ , with  $\beta \gg 1$ . For JJs with the same thickness but different junction area  $\{A_j\}$ ,  $E_{J,j} \propto A_j$  and  $C_j \propto A_j$ . The charging energies can be defined as  $E_{C,1} = E_{C,2} = E_C = \frac{e^2}{2C_1}$ ,  $E_{C,3} = \alpha^{-1} E_C$  and  $E_{C,4} = \beta^{-1} E_C$ . Notice that  $E_{J,j} E_{C,j} = E_J E_C$  is independent of  $j$ . The system may have two stable states with persistent circulating current of opposite sign.

Here is a summary of the key results:

1. For  $\beta \rightarrow \infty$ , we may neglect the fourth JJ and reduce the system to the well-studied flux qubit with three JJs [15, 19]. For  $\beta \gg 1$ , there is only a small phase difference across the fourth junction, with  $\theta_4 = \pm \theta_4^* = \mathbf{Z}_{\text{flux}} \theta_4^*$  depending on the sign of the circulating current (i.e., the state of flux qubit, with  $\mathbf{Z}_{\text{flux}} = (|0\rangle\langle 0| - |1\rangle\langle 1|)_{\text{flux}}$ ). We show that the magnitude of the phase difference can be small  $\theta_4^* \approx \frac{\sqrt{4\alpha^2 - 1}}{2\alpha\beta} \propto \beta^{-1}$ . As shown in Fig. 4, two SC islands ( $c$  and  $d$ ) are connected by this junction, if we fix the SC phase  $\phi_c$ , then  $\phi_d = \varepsilon^{0,1} = \phi_c \pm \theta_4^*$  has phase separation  $\Delta\varepsilon = 2\theta_4^* \approx \frac{\sqrt{4\alpha^2 - 1}}{\alpha\beta}$ . The SC island  $d$  can be used to coherently control the coupling between the Majorana fermions of the STIS wire.

2. There are quantum fluctuations for the phase of the SC island. The magnitude of quantum fluctuations depends on  $\{E_{C,j}\}$  and  $\{E_{J,j}\}$ . For  $\beta \gg 1$ , the dynamics associated with  $\theta_4$  can be characterized by a harmonic

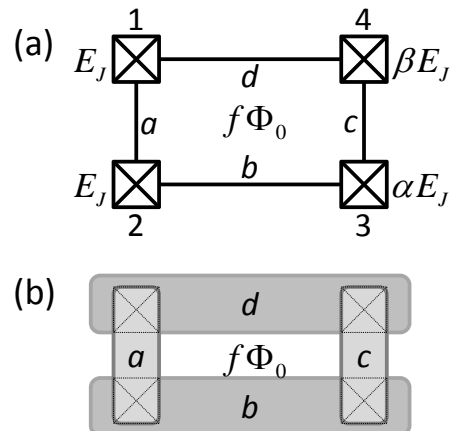


FIG. 4: The design of flux qubit consists of a loop of four JJs in series that encloses an external magnetic flux  $f\Phi_0$ . Schematic illustration in terms of (a) JJs and (b) SC islands.

oscillator (HO) Hamiltonian

$$H^{\text{HO}} = \frac{p_{\theta_4}^2}{2M_4} + \frac{E_{J,4}}{2} (\theta_4 - \mathbf{Z}_{\text{flux}} \theta_4^*)^2,$$

where the effective mass is  $M_4 = \frac{1}{8E_{c4}}$  and the canonical momentum  $p_{\theta_4}$  satisfies  $[\theta_4, p_{\theta_4}] = i$  (with  $\hbar \equiv 1$ ). We may rewrite  $H^{\text{HO}} = (a^\dagger a + 1/2) \omega$  and  $\theta_4 = \mathbf{Z}_{\text{flux}} \theta_4^* + \zeta (a^\dagger + a) / \sqrt{2}$ , where the oscillator frequency is  $\omega = \sqrt{8E_J E_C}$  and the magnitude of quantum fluctuations is  $\zeta = \left(\frac{8E_C}{E_J}\right)^{1/4} \beta^{-1/2}$ . We justify that this simple model agrees very well with the general model characterizing the quantum fluctuations for the flux qubit with coupled JJs.

3. Various parameters characterizing the flux qubit are also calculated, including the plasma frequencies  $\{\omega_i\}_{i=1,2,3}$ , barrier height  $\Delta U$ , and the tunneling matrix element  $t$ . For example, given parameters  $\alpha = 0.8$  and  $\beta = 10$ , we compute  $\{\omega_i\} \approx (2.8, 2.3, 1.8) \sqrt{E_J E_C} \sim \sqrt{E_J E_C}$ ,  $\Delta U \approx 0.26 E_J$ , and  $t \approx 1.8 \sqrt{E_J E_C} \exp[-0.7 (E_J/E_C)^{1/2}]$ . We notice that these parameters for the flux qubit hardly depend on  $\beta$  when  $\beta > 10$ , which verifies the intuition that inserting a large Josephson junction to the loop has almost no effect to the properties of the flux qubit.

4. We propose two schemes to implement the SC phase-controller, which can fix the phase difference between an SC island and a big SC reservoir.

In the following, we provide detailed analysis to justify our design of flux qubit with four JJs. First, we give the Hamiltonian description for the system. Then, we calculate the phase separation and quantum fluctuations. Next, we numerically obtain various quantities such as plasma frequencies, barrier height, and tunneling matrix element. Our numerical calculation also verifies our estimates on phase separation and magnitude of quantum fluctuations. After that, we propose two implementations of the SC phase-controller. Finally, we derive the energy splitting function  $E(\varepsilon)$  that is highly non-linear in terms of  $\varepsilon$ .

## Appendix B: Hamiltonian for Flux Qubit

The Hamiltonian for a flux qubit consisting of four JJs in series is

$$H^{\text{flux}} = T + U, \quad (\text{B1})$$

with the Josephson potential

$$U = \sum_{j=1,2,3,4} E_{J,j} (1 - \cos \theta_j), \quad (\text{B2})$$

and the capacitive charging energy

$$T = \frac{1}{2} \sum_{j=1,2,3,4} C_j V_j^2. \quad (\text{B3})$$

Here for the  $j$ -th Josephson junction,  $E_{J,j}$  is the Josephson coupling,  $\theta_j$  is the gauge-invariant phase difference,  $C_j$  is the capacitance, and  $V_j$  is the voltage across the junction. Suppose that all the junctions have the same thickness, we have  $E_{J,j} \propto A_j$  and  $E_{C,j} \equiv \frac{e^2}{2C_j} \propto A_j^{-1}$  where  $A_j$  is the area of the junction and  $C_j$  is the junction capacitance [16]. The quantity  $E_{J,j} E_{C,j} = E_J E_C$  does not depend on  $j$ .

The Josephson potential is constraint by the phase relation

$$\sum_j \theta_j + 2f\pi \equiv 0 \pmod{2\pi}, \quad (\text{B4})$$

This phase relation removes one degree of freedom. We may introduce a 3-vector  $\vec{\theta} = (\theta_1, \theta_2, \theta_3)$  to characterize the system with four JJs. (Note that we only need to choose three independent phases for 3-vector, e.g.,  $\vec{\theta} = (\theta_1, \theta_2, \theta_4)$  is also a valid choice.) For  $f = 1/2$ , the Josephson potential is

$$U = -E_{J,1} \cos \theta_1 - E_{J,2} \cos \theta_2 - E_{J,3} \cos \theta_3 + E_{J,4} \cos(\theta_1 + \theta_2 + \theta_3). \quad (\text{B5})$$

By appropriately choosing the parameter  $\{E_{J,j}\}$ , there are only two minima for the Josephson energy at  $\pm \{\theta_j^*\} = \pm \{\theta_1^*, \theta_2^*, \theta_3^*, \theta_4^*\}$  (see Fig. 5ab). We may identify the two levels of the flux qubit as  $|0\rangle_{\text{flux}} = |\{\theta_i^*\}\rangle$  and  $|1\rangle_{\text{flux}} = |{-\theta_i^*}\rangle$ . Thus, we may denote the two potential minima as  $\{\mathbf{Z}_{\text{flux}} \theta_j^*\}$ , with  $\mathbf{Z}_{\text{flux}} = (|0\rangle\langle 0| - |1\rangle\langle 1|)_{\text{flux}}$ .

The capacitive charging energy can be regarded as the kinetic energy associated with the dynamics of  $\vec{\theta}$ . This is because the voltage across the junction is given by the Josephson voltage-phase relation  $V_j = \left(\frac{\Phi_0}{2\pi}\right) \dot{\theta}_j$  [16] and the time derivatives  $\{\dot{\theta}_j\}$  obey the constraint  $\dot{\theta}_1 + \dot{\theta}_2 + \dot{\theta}_3 + \dot{\theta}_4 = 0$  (derived from Eq.(B4)). Thus, we may write the capacitive charging energy as

$$T = \frac{1}{2} \left(\frac{\Phi_0}{2\pi}\right)^2 \sum_{i,j=1,2,3} C_{ij} \dot{\theta}_i \dot{\theta}_j \quad (\text{B6})$$

$$= \frac{1}{2} \vec{\dot{\theta}}^T \cdot \mathbf{M} \cdot \vec{\dot{\theta}} \quad (\text{B7})$$

$$= \frac{1}{2} \vec{p}^T \cdot \mathbf{M}^{-1} \cdot \vec{p}, \quad (\text{B8})$$

where the capacitive matrix is

$$C_{ij} = C_i \delta_{ij} + C_4, \quad (\text{B9})$$

the effective mass tensor is

$$\mathbf{M} = \left(\frac{\Phi_0}{2\pi}\right)^2 \mathbf{C}, \quad (\text{B10})$$

and the canonical momentum is

$$\vec{p} = \mathbf{M} \cdot \vec{\dot{\theta}}. \quad (\text{B11})$$



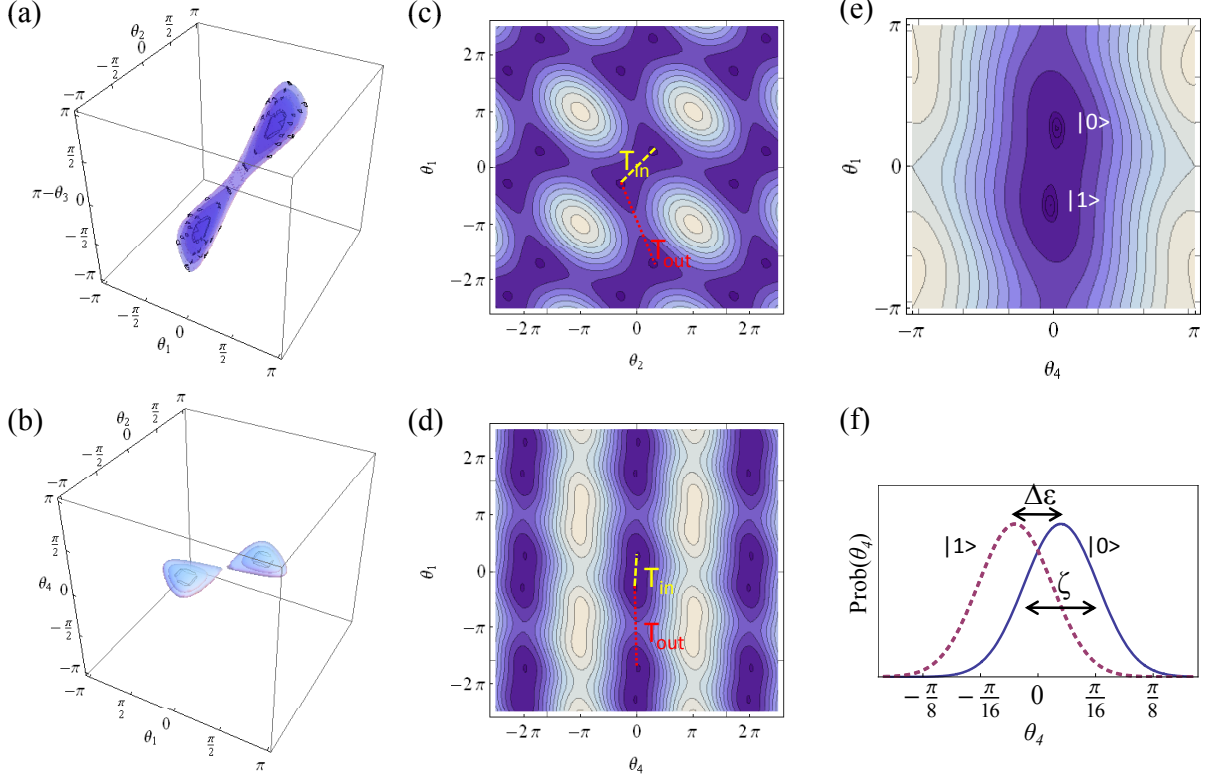


FIG. 5: Contour plots of Josephson energy as a function of (a)  $\{\theta_1, \theta_2, \theta_3\}$  (with  $\theta_4 = \pi - \theta_1 - \theta_2 - \theta_3$ ). (b)  $\{\theta_1, \theta_2, \theta_4\}$  (with  $\theta_3 = \pi - \theta_1 - \theta_2 - \theta_4$ ). (c)  $\{\theta_1, \theta_4\}$  (with  $\theta_3 = \pi - \theta_1 - \theta_2$  and  $\theta_4 = 0$ ) (d,e)  $\{\theta_1, \theta_4\}$  (with  $\theta_1 = \theta_2$  and  $\theta_3 = \pi - 2\theta_1 - \theta_4$ ). (f) Marginal probability distributions of  $\theta_4$  associated with states  $|0\rangle_{\text{flux}}$  (blue solid line) and  $|1\rangle_{\text{flux}}$  (red dashed line). The parameters are  $E_J/E_C = 80$  and  $\{E_{J,i}/E_J\}_{i=1,2,3,4} = \{1, 1, \alpha = 0.8, \beta = 10\}$ .

Therefore, we have reduced the problem to the canonical model of the quantum system with Hamiltonian

$$H = \frac{1}{2} \vec{p}^T \cdot \mathbf{M}^{-1} \cdot \vec{p} + U(\vec{\theta}), \quad (\text{B12})$$

where the operators satisfy the commutation relation  $[\theta_j, p_k] = i\delta_{jk}$ .

Based on this model, we obtain the phase separation and the magnitude of quantum fluctuations in the next two sections.

### Appendix C: Phase Separation between the Potential Minima

We now calculate the potential minimum  $\{\theta_j^*\}$  by introducing a Lagrange variable  $\lambda$  associated with the phase relation (Eq.(B4)). We study the function

$$F = - \sum_{j=1,2,3,4} E_{J,j} \cos \theta_j - \lambda \left( \sum_j \theta_j - \pi \right). \quad (\text{C1})$$

The first derivatives all vanish at the extreme point:

$$E_{J,j} \sin \theta_j^* = \lambda. \quad (\text{C2})$$

From the phase relation  $\sum_j \theta_j^* = \sum_j \sin^{-1} \frac{\lambda}{E_{J,j}} = \pi$ , we may solve for  $\lambda$ .

For our system with four JJs, we can also calculate  $\theta_4^*$  by series expansion with respect to the small parameter  $\beta^{-1}$ . For  $\beta \rightarrow \infty$ , we have the zeroth order expansion  $\lambda^{(0)} = \frac{\sqrt{4\alpha^2 - 1}}{2\alpha}$ ,  $\theta_1^{(0)} = \theta_2^{(0)} = \sin^{-1} \lambda^{(0)} = \cos^{-1} \frac{1}{2\alpha}$ ,  $\theta_3^{(0)} = \pi - 2 \cos^{-1} \frac{1}{2\alpha}$  and  $\theta_4^{(0)} = 0$ . Then, to the first order of  $\beta^{-1}$ , we have  $\theta_4^{(1)} = \sin^{-1} \frac{\lambda^{(0)}}{\beta} \approx \frac{\sqrt{4\alpha^2 - 1}}{2\alpha\beta}$ . Therefore, the phase difference for the fourth junction is

$$\theta_4^* = \frac{\sqrt{4\alpha^2 - 1}}{2\alpha\beta} + (\beta^{-2}). \quad (\text{C3})$$

As plotted in Fig. 6b, the numerically obtained quantity  $\frac{1}{\Delta\varepsilon} = \frac{1}{2\theta_4^*} \propto \beta$ .

### Appendix D: Models for Quantum Fluctuations of the SC Phase

In this section, we consider two models for quantum fluctuations across the JJs. The quantum fluctuations across the JJs are due to the finite mass matrix for the Hamiltonian (Eq.(B12)), which is proportional to the ca-

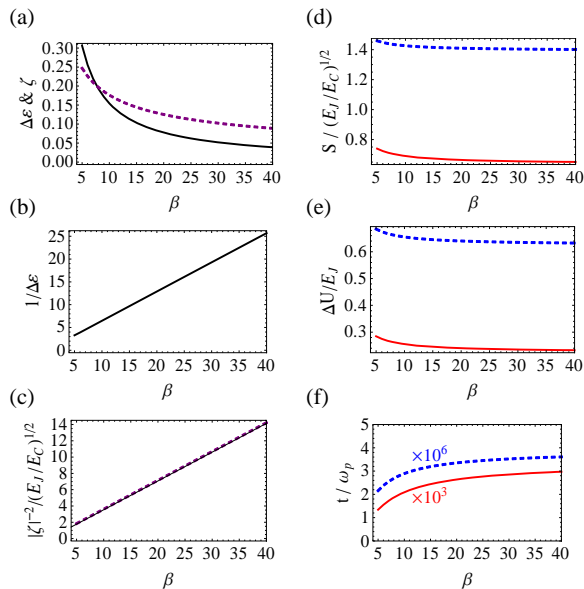


FIG. 6: Parameters for the flux qubit as a function of  $\beta$ . (a,b,c) Phase separation  $\Delta\epsilon$  (dark solid line) and the magnitude of quantum fluctuations  $\zeta$  (purple dashed line) from numerical calculation. The theoretical prediction from Eq. (D3) (gray solid line in (c)) agrees very well with the numerical calculation. (d,e,f) The two ground states of the flux qubit can be coupled by intra-cell tunneling (red solid lines) and inter-cell tunneling (blue dashed lines) [15, 19], characterized by the action  $S$ , potential barrier  $\Delta U$ , and tunneling rate  $t$ . Panels (a) and (f) assume  $E_J/E_C = 80$ .

capacitance matrix. In the following, we first provide a simple, intuitive model to characterize the quantum fluctuations associated with  $\theta_4$  for  $\beta \gg 1$ . Then, we consider the general model of multiple coupled harmonic oscillators, and obtain the formula for the magnitude of quantum fluctuations associated with a projected degree of freedom. We find very good agreement between the two models when  $\beta \gg 1$ , which justifies the simple model.

### 1. Simple Model – One Harmonic Oscillator

Given very large  $\beta$ , we may neglect the higher order couplings to other JJs and consider the reduced Hamiltonian for the fourth JJ

$$H_{J,4} = \frac{1}{2}C_4V_4^2 + E_{J,4}(1 - \cos(\theta_4 - \mathbf{Z}_{\text{flux}}\theta_4^*)), \quad (\text{D1})$$

with displaced potential minimum at  $\mathbf{Z}_{\text{flux}}\theta_4^*$ . We then use the harmonic approximation and obtain

$$H^{\text{HO}} = \frac{p_{\theta_4}^2}{2M_4} + \frac{E_{J,4}}{2}(\theta_4 - \mathbf{Z}_{\text{flux}}\theta_4^*)^2, \quad (\text{D2})$$

where  $M_4 = \frac{1}{8E_{C,4}}$  and  $E_{C,4} = \frac{e^2}{2C_4}$ . The oscillator has frequency  $\omega = \sqrt{8E_{J,4}E_{C,4}} = \sqrt{8E_JE_C}$  and characteris-

tic length

$$\zeta = \left(\frac{8E_{C,4}}{E_{J,4}}\right)^{1/4} = \left(\frac{8E_C}{E_J}\right)^{1/4} \beta^{-1/2}. \quad (\text{D3})$$

Here  $\zeta$  is also the magnitude of quantum fluctuations.

### 2. General Model – Coupled Harmonic Oscillators

We now consider the general model of multiple coupled harmonic oscillators, and obtain the formula for the magnitude of quantum fluctuations associated with a projected degree of freedom.

Close to the potential minimum  $\{\mathbf{Z}_{\text{flux}}\theta_j^*\}$ , we may expand the potential function to the second order of  $\vec{x} \equiv \vec{\theta} - \mathbf{Z}_{\text{flux}}\vec{\theta}^*$

$$U = U_{\min} + \frac{1}{2} \sum_{i,j=1,2,3} K_{ij}x_ix_j + O(x^3) \quad (\text{D4})$$

with

$$K_{ij} = \left. \frac{d^2U}{d\theta_id\theta_j} \right|_{\vec{\theta}=\vec{\theta}^*}. \quad (\text{D5})$$

The effective Hamiltonian around the minimum describes a system of coupled Harmonic oscillators:

$$H_{\text{oscillator}} = \frac{1}{2} \sum_{i,j=1,2,3} M_{ij}\dot{x}_i\dot{x}_j + \frac{1}{2} \sum_{i,j=1,2,3} K_{ij}x_ix_j \quad (\text{D6})$$

$$= \frac{1}{2}\vec{p}^T \cdot \mathbf{M}^{-1} \cdot \vec{p} + \frac{1}{2}\vec{x}^T \cdot \mathbf{K} \cdot \vec{x} \quad (\text{D7})$$

where we have used the definition  $\vec{p} = \mathbf{M} \cdot \dot{\vec{\theta}} = \mathbf{M} \cdot \dot{\vec{x}}$ .

To solve for the system of coupled oscillators, we perform the following transformation to make the mass matrix/tensor isotropic. For real and symmetric mass matrix ( $M_{ij} = M_{ji}$ ), there is an orthogonal transformation  $V_1$  (with  $V_1^{-1} = V_1^T$ ) that diagonalizes the mass matrix

$$V_1\mathbf{M}V_1^T = \mathbf{\Lambda} \quad (\text{D8})$$

where  $\Lambda_{ij} = \lambda_i\delta_{ij}$  is the diagonal matrix. The eigenvalue  $\lambda_i$  is effective mass along the  $i$ -th principle axis. By inverting both sides, we have  $V_1\mathbf{M}^{-1}V_1^T = \mathbf{\Lambda}^{-1}$ . For diagonal matrix, we may also define  $(\Lambda^{\pm 1/2})_{ij} = \lambda_i^{\pm 1/2}\delta_{ij}$ . Introducing the transformation

$$\vec{x}' = \Lambda^{1/2}V_1 \cdot \vec{x} \quad (\text{D9})$$

$$\vec{p}' = \Lambda^{-1/2}V_1 \cdot \vec{p} \quad (\text{D10})$$

we have

$$H_{\text{oscillator}} = \frac{1}{2}\vec{p}'^T \cdot \vec{p}' + \frac{1}{2}\vec{x}'^T \cdot \tilde{\mathbf{K}} \cdot \vec{x}' \quad (\text{D11})$$



where

$$\tilde{\mathbf{K}} = \Lambda^{-1/2} (V_1 K V_1^T) \Lambda^{-1/2}. \quad (\text{D12})$$

Finally, we diagonalize the real symmetric matrix  $\tilde{\mathbf{K}}$  via orthogonal transformation  $V_2$

$$V_2 \tilde{\mathbf{K}} V_2^T = \Omega \quad (\text{D13})$$

where  $\Omega_{ij} = \omega_i^2 \delta_{ij}$  is the diagonal matrix. Overall, the position and momentum transform as

$$\vec{y} = V_2 \vec{x}' = V_2 \Lambda^{1/2} V_1 \cdot \vec{x} \quad (\text{D14a})$$

$$\vec{q} = V_2 \vec{p}' = V_2 \Lambda^{-1/2} V_1 \cdot \vec{p} \quad (\text{D14b})$$

The eigenvalue  $\omega_i^2$  is the square of the  $i$ -th oscillator frequency (also called plasma frequency). Given parameters  $\alpha = 0.8$  and  $\beta = 10$ , we calculate the plasma frequencies  $\{\omega_i\}_{i=1,2,3} = \{2.8, 2.3, 1.8\} \sqrt{E_J E_C}$ . We may also vary the parameter  $\beta$ , and observe that the plasma frequencies only depend very weakly for  $\beta \gg 1$ .

Note that position and momentum have different transformations  $V_2 \Lambda^{1/2} V_1$  and  $V_2 \Lambda^{-1/2} V_1$ . Furthermore, these transformations are not orthogonal transformations. However, as long as the transformations preserve the commutation relation  $[\hat{y}_j, \hat{q}_k] = [\hat{x}_j, \hat{p}_k] = i\delta_{jk}$ , we can still perform quantization over the transformed coordinate.

Following this procedure, we can numerically compute the magnitude of quantum fluctuations of  $\theta_4$  as detailed below.

### 3. Quantum Fluctuations in SC Phase

We now quantize the phase difference across the fourth junction  $\theta_4$ . Near the potential minimum at  $\{\theta_i^*\}$ , we perform the transformation of Eq. (D14) along with the quantization  $\hat{y}_i = \frac{\hat{a}_i^\dagger + \hat{a}_i}{\sqrt{2}}$  and  $\hat{q}_i = \frac{\hat{a}_i^\dagger - \hat{a}_i}{\sqrt{2}i}$ , we obtain the Hamiltonian for three uncoupled harmonic oscillators

$$\tilde{H}_{\text{oscillator}} = \sum_{i=1,2,3} \hbar \omega_i \left( \hat{a}_i^\dagger \hat{a}_i + \frac{1}{2} \right), \quad (\text{D15})$$

with eigenfrequencies of  $\{\omega_i\}_{i=1,2,3}$ . Each oscillatory mode may induce quantum fluctuations in  $\theta_4$ , with characteristic length scale  $\zeta_i$ . The operator form of  $\theta_4$  can be written as

$$\theta_4 = \mathbf{Z}_{\text{flux}} \theta_4^* + \sum_{i=1,2,3} \zeta_i \frac{\hat{a}_i^\dagger + \hat{a}_i}{\sqrt{2}} \quad (\text{D16})$$

We calculate the values of  $\zeta_i$  as the following. In the  $y$ -coordinate, the characteristic displacement vector for the  $i$ -th mode is  $\vec{l}_i^{(y)} = \sqrt{\frac{\hbar}{\omega_i}} \vec{e}_i^{(y)}$ , with unit vector  $\vec{e}_i$  along the  $i$ -th direction. We may transform this back to the  $x$ -coordinate,  $\vec{l}_i^{(x)} = (V_2 \Lambda^{1/2} V_1)^{-1} \cdot \sqrt{\frac{\hbar}{\omega_i}} \vec{e}_i^{(y)}$ . Note that

$\vec{l}_i^{(x)}$  is no longer orthogonal. From  $\vec{l}_i^{(x)}$ , we can obtain the characteristic fluctuating scale of  $\zeta_i = \left| \sum_{k=1,2,3} \left( \vec{l}_i^{(x)} \right)_k \right|$ . The magnitude of quantum fluctuations of  $\theta_4$  can be computed as

$$\zeta = \left( \sum_{i=1,2,3} |\zeta_i^2| \right)^{1/2} \quad (\text{D17})$$

for independent fluctuations from the three uncoupled harmonic oscillators.

As plotted in Fig. 6c, the numerically obtained value for  $\zeta$  (using Eq. (D17)) agrees very well with the prediction from the simple model (using Eq. (D3)), which scales as  $\beta^{-1/2}$ . Therefore, the simple model of Eq. (D3) provides a reliable description to characterize the dynamics associated with  $\theta_4$ .

## Appendix E: Tunneling Matrix Element

### 1. WKB method

We use the WKB method to estimate the tunneling matrix element [19]. The action associated with the pathway  $\vec{\theta}(r)$  from  $\vec{\theta}(0) = \vec{\theta}_a$  to  $\vec{\theta}(1) = \vec{\theta}_b$  is

$$S = \int_{\vec{\theta}_a}^{\vec{\theta}_b} \sqrt{2(U-E)} \sqrt{d\vec{\theta}^T \cdot \mathbf{M} \cdot d\vec{\theta}}, \quad (\text{E1})$$

and the tunneling matrix element can be estimated as

$$t \approx \frac{\hbar \omega}{2\pi} e^{-S/\hbar}. \quad (\text{E2})$$

The phase space  $\vec{\theta}$  has period  $2\pi$  for all three directions. We may introduce the unit cell with volume  $(2\pi)^3$  and three basis vectors  $\vec{a}_1 = 2\pi(1, 0, 0)$ ,  $\vec{a}_2 = 2\pi(0, 1, 0)$ , and  $\vec{a}_3 = 2\pi(0, 0, 1)$ . (Note that we may choose the shape of the unit cell for our convenience.) Regarding the tunneling pathway, we may choose the initial point  $\vec{\theta}_a^* = -\vec{\theta}^*$ , while the choice for final point is not unique as  $\vec{\theta}_b = \vec{\theta}^* + \sum_i n_i \vec{a}_i$  for integers  $\{n_i\}$ . However, we may require that the final point,  $\vec{\theta}_b^*$ , be the one that has the minimum action from the initial point, and we choose the unit cell so that it includes the minimum action pathway that connects  $\vec{\theta}_a^*$  and  $\vec{\theta}_b^*$ . After this procedure, the intra-cell tunneling has the minimum action, compared to all inter-cell tunneling pathways.

### 2. Pathway with minimum action

We should use the pathway  $\vec{\theta}(r)$  with extreme action for the WKB method, i.e.,

$$\frac{\delta S}{\delta \vec{\theta}(r)} = 0.$$

We obtain these extreme pathways using the following approach. First, we discretize the integration

$$S = \sum_{i=1}^N |\vec{x}_i - \vec{x}_{i-1}| f\left(\frac{\vec{x}_i + \vec{x}_{i-1}}{2}\right), \quad (\text{E3})$$

with  $\vec{x}_0 = \vec{\theta}_a$  and  $\vec{x}_N = \vec{\theta}_b$ . Then we calculate the derivatives with respect to  $\vec{r}_i$

$$\begin{aligned} \frac{\delta S}{\delta \vec{r}_i} &= \frac{\Delta \vec{x}_i}{|\Delta \vec{x}_i|} f\left(\frac{\vec{x}_i + \vec{x}_{i-1}}{2}\right) - \frac{\Delta \vec{x}_{i+1}}{|\Delta \vec{x}_{i+1}|} f\left(\frac{\vec{x}_{i+1} + \vec{x}_i}{2}\right) \\ &+ |\Delta \vec{x}_i| \nabla f\left(\frac{\vec{x}_i + \vec{x}_{i-1}}{2}\right) + |\Delta \vec{x}_{i+1}| \nabla f\left(\frac{\vec{x}_{i+1} + \vec{x}_i}{2}\right). \end{aligned} \quad (\text{E4})$$

For extreme pathway, these derivatives should vanish. If we start with a non-extreme pathway with non-vanishing derivatives, we can update the pathway so that the updated pathway becomes closer to the extreme pathway. By repeating the update procedure many times, we will obtain a pathway that is very close to the extreme pathway. Since we know in advance that we are looking for the pathway that gives the minimum action, we apply the following update rules for the  $k$ th update:

$$\vec{r}_i^{(k+1)} = \vec{r}_i^{(k)} - \epsilon \frac{\delta S}{\delta \vec{r}_i} \quad (\text{E5})$$

where  $\epsilon$  determines the evolution rate and  $i = 1, 2, \dots, N-1$ . For sufficiently small evolution rate

$$S\left[\left\{\vec{r}_i^{(k+1)}\right\}\right] - S\left[\left\{\vec{r}_i^{(k)}\right\}\right] = -\epsilon \left(\frac{\delta S}{\delta \vec{r}_i}\right)^2 + O(\epsilon^2) \leq 0, \quad (\text{E6})$$

which ensures continuous reduction of the action.

### 3. Tunneling rates and $\beta$ Dependence

This algorithm gives us the correct pathway that locally minimize the action between neighboring potential wells. We find that the pathways are essentially the straight lines connecting the different minima, with no significant difference in terms of the action values. For example, given parameters  $\alpha = 0.8$  and  $\beta = 10$ , the intra-cell action is  $S_{in} \approx 0.7\hbar\sqrt{E_J/E_C}$  and the smallest inter-cell action is  $S_{out} \approx 1.4\hbar\sqrt{E_J/E_C}$ . For  $E_J/E_C \approx 80$ , we will have  $t_2/t_1 \approx \exp[(S_1 - S_2)/\hbar] \sim 10^{-3} \ll 1$ . The barrier height for intra-cell tunneling is  $\Delta U = 0.25E_J$ .

When  $\beta \rightarrow \infty$ , all quantities (potential minimum position, plasma frequencies, action for tunneling, energy barrier, and tunneling matrix element) reduce to the case with three JJs. As illustrated in Fig. 6, the deviation scales as  $\beta^{-1}$ . For  $\beta \geq 10$ , the perturbation from  $\beta$  is very small.

For practical parameters of mesoscopic aluminum junctions with critical current density 500 A/cm<sup>2</sup> [15, 19], a junction with an area of  $A = 0.2 \times 0.4 \mu\text{m}^2$  can achieve

$E_J \approx 200$  GHz and  $E_J/E_C \approx 80$ , which corresponds to the first two junctions  $E_{J,1} = E_{J,2} = E_J$ . Since  $E_{J,j} \propto A_j$ , the fourth junction  $E_{J,4} = \beta E_J$  should have an area of approximately  $1 \times 1 \mu\text{m}^2$  to achieve  $\beta \approx 10$ .

## Appendix F: Phase-Controllers

For the STIS quantum wire, we would like to fix the phase difference between two disconnected SC islands. For example, we would like have  $\phi_l - \phi_u = \pi/2$ ,  $\phi_r - \phi_u = \pi/2$ ,  $\phi_c - \phi_u = \phi_c + \pi$ , as shown in Fig. 1ac. The idea is to connect the two SC islands via a phase-controller. The phase-controller has two large SC islands with a controllable phase difference  $\gamma$ . Using large SC islands for phase-controllers reduces quantum fluctuations in the SC phase.

In this section, we consider two approaches to building a phase-controller using Josephson junctions (JJs). The phase difference  $\gamma$  between the two large SC islands can be controlled by either the external magnetic flux  $\gamma = \gamma(\Phi_x)$  or the electric current  $\gamma = \gamma(I)$ , as detailed below.

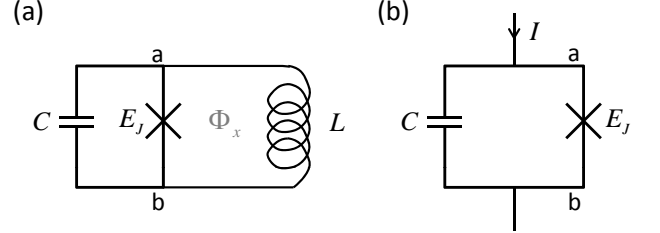


FIG. 7: The phase-controllers can establish desired phase difference  $\gamma$  between SC islands  $a$  and  $b$ . For example, (a) the flux phase-controller with external magnetic flux  $\Phi_x$ , and (b) the current phase-controller with external electric current  $I$ .

### 1. Flux phase-controller

The *flux phase-controller* uses an rf SQUID loop that is interrupted by a single Josephson junction (Fig. 7a). We may change the external magnetic flux enclosed by the loop, to induce the desired phase difference between the two SC islands,  $a$  and  $b$ . The rf SQUID loop has inductance  $L$ , and the JJ has Josephson coupling energy  $E_J$  and capacitive charging energy  $E_C (= e^2/2C)$ . The Hamiltonian for the flux phase-controller is

$$H = U + T, \quad (\text{F1})$$

where the potential energy is

$$U = \frac{1}{2L} \left( \Phi_x - \frac{\Phi_0}{2\pi} \gamma \right)^2 + E_J (1 - \cos \gamma) \quad (\text{F2})$$

with  $\Phi_x$  for the external flux enclosed by the loop and  $\gamma$  for the gauge invariant phase difference across the junction, and the capacitive charging energy is

$$T = \frac{1}{2}CV^2 \quad (\text{F3})$$

with the voltage  $V = \frac{\Phi_0}{2\pi} \frac{d\gamma}{dt}$  and the effective mass  $m_{eff} = C \left(\frac{\Phi_0}{2\pi}\right)^2$ .

We find that the potential minimum satisfies the condition

$$\Phi_x = \frac{\Phi_0}{2\pi}\gamma + E_J L \frac{2\pi}{\Phi_0} \sin \gamma, \quad (\text{F4})$$

This expression can be used to determine  $\gamma$  as a function of  $\Phi_x$ . For  $L \rightarrow 0$ , we have  $\gamma = -2\pi \frac{\Phi_x}{\Phi_0}$ . For sufficiently small  $L$  (satisfying  $L < \frac{\Phi_0^2}{4\pi^2 E_J}$ ), this relation is still single valued for all  $\gamma$ . Therefore, we can deterministically control the gauge invariant phase difference  $\gamma$  by applying an appropriate  $\Phi_x$ .

We then consider the perturbation around the potential minimum and obtain the plasma frequency  $\omega_p \approx (LC)^{-1/2}$  for  $L \ll \frac{\Phi_0^2}{4\pi^2 E_J}$ . The quantum fluctuations of  $\gamma$  around the potential minimum has characteristic scale

$$\zeta_{\text{flux}} = \sqrt{\frac{\hbar}{m_{eff}\omega_p}} \approx 2\sqrt{\pi} \left(\frac{E_c}{E_L}\right)^{1/4}. \quad (\text{F5})$$

## 2. Current phase-controller

Alternatively, we may also control the phase differences via the external current  $I$  through a Josephson junction (Fig. 7a). The Hamiltonian for such a *current phase-controller* is

$$H = U + T, \quad (\text{F6})$$

where the potential energy is

$$U = -I \frac{\Phi_0}{2\pi} \gamma + E_J (1 - \cos \gamma) \quad (\text{F7})$$

with  $\gamma$  for the gauge invariant phase difference across the junction, and the capacitive charging energy is

$$T = \frac{1}{2}CV^2 \quad (\text{F8})$$

with the voltage  $V = \frac{\Phi_0}{2\pi} \frac{d\gamma}{dt}$  and the effective mass  $m_{eff} = C \left(\frac{\Phi_0}{2\pi}\right)^2$ .

As long as  $I < I_c \equiv \frac{2\pi}{\Phi_0} E_J$ , we have the potential minimum at

$$\gamma = \sin^{-1} I/I_c. \quad (\text{F9})$$

We then consider the perturbation around the potential minimum and obtain the plasma frequency  $\omega_p \approx$

$\left(\frac{2eI_c \cos \gamma^*}{\hbar C}\right)^{1/2}$ . The quantum fluctuations of  $\gamma$  around the potential minimum has characteristic scale

$$\zeta_{\text{current}} = \sqrt{\frac{\hbar}{m_{eff}\omega_p}} = \left(\frac{8}{\cos \gamma^*} \frac{E_c}{E_J}\right)^{1/4}. \quad (\text{F10})$$

## 3. Comparison between flux and current phase-controllers

Both flux and current phase-controllers enable us to reliably induce phase difference between two SC islands. We compare the two phase-controllers in the following aspects:

(1) Tunable phase rage: A single flux phase-controller can create all desired phase differences in the range  $[-\pi, \pi]$ . In contrast, a single current phase-controller can only create phase difference in the range  $(-\pi/2, \pi/2)$ . However, by using two or more current phase-controllers in series, it is possible to create arbitrary phase differences.

(2) Quantum fluctuations: Both controllers have similar scaling for the quantum fluctuations, which scales as  $(E_c/E_{L,J})^{1/4}$ . In order to minimize the quantum fluctuations, we may use the JJ loops with a small inductance (i.e.,  $E_L > E_J$ ) for flux phase-controller, while we may use the JJ loops with large Josephson coupling energy  $E_J$  for current phase-controller. Note that for current phase-controller the quantum fluctuations becomes unfavorably large when  $\gamma \approx \pi/2$ , which can be overcome by using two or more controllers in series to reduce the fluctuations.

## 4. Parameters

We may estimate the quantum fluctuations for practical devices. According to the experimental parameters of the large Josephson junctions [21]: the charging energy  $E_c \equiv e^2/2C = 0.15$  mK and the Josephson coupling energy  $E_J = I_c \Phi_0/2\pi = 500$  K, which gives us  $\zeta_{\text{current}} \approx (8 * \frac{0.00015}{500})^{1/4} = 0.04$ . It is also possible to build a SQUID loop with very small inductive energy  $E_L \equiv \Phi_0^2/2L = 645$  K [25], and we can obtain  $\zeta_{\text{flux}} \approx 2\sqrt{\pi} * (\frac{0.00015}{645})^{1/4} \approx 0.08$ . By further increasing the junction area, we may further decrease  $E_c$  and increase  $E_J$ , which should give us more reduced quantum fluctuations from the phase-controller.

## Appendix G: Brief Derivation for Energy Splitting $E(\varepsilon)$

We now briefly derive the energy splitting function  $E(\varepsilon)$ , which is a highly non-linear function of  $\varepsilon$ . The derivation mostly follows Ref. [5].

We start with the effective Hamiltonian [5]

$$H^{\text{STIS}} = -iv_F\tau^x\partial_x + \delta_\varepsilon\tau^z, \quad (\text{G1})$$

with  $\delta_\varepsilon = -\Delta_0 \sin \varepsilon/2$  (differed from [5] by a minus sign, due to a slightly different assignment of SC phases). The Hamiltonian can be written as

$$H^{\text{STIS}}(k) = v_F k \tau^x + \delta_\varepsilon \tau^z = \begin{pmatrix} \delta_\varepsilon & v_F k \\ v_F k & -\delta_\varepsilon \end{pmatrix}, \quad (\text{G2})$$

where  $k$  is the wave vector in the quantum wire. The eigen-energies for  $H^{\text{STIS}}(k)$  are  $E^\pm(\delta_\varepsilon, k) = \pm\sqrt{\delta_\varepsilon^2 + v_F^2 k^2}$ . For a finite STIS quantum wire with length  $L$ , it can only support a discretized set of wave vectors satisfying the boundary condition [5]

$$\tan kL = -\frac{v_F k}{\delta_\varepsilon} = kL/\Lambda_\varepsilon, \quad (\text{G3})$$

with a dimensionless parameter

$$\Lambda_\varepsilon \equiv -\delta_\varepsilon L/v_F. \quad (\text{G4})$$

For given  $\Lambda_\varepsilon$ , we may solve Eq. (G3) and obtain a set of solutions  $kL = f_n(\Lambda_\varepsilon)$  with index  $n = 0, 1, 2, \dots$  for different bands. The function  $f_n(y)$  is just the inverse function of  $y = x/\tan(x)$  associated with the  $n$ th invertible domain.

For the lowest band, we have

$$E(\varepsilon) \equiv E^+(\delta_\varepsilon, k_0) = \Delta E \sqrt{\Lambda_\varepsilon^2 + f_0^2(\Lambda_\varepsilon)}, \quad (\text{G5})$$

with  $\Delta E = v_F/L$ . Note that  $kL = f_0(\Lambda_\varepsilon)$  is purely imaginary for  $\Lambda_\varepsilon \in (1, \infty)$ , and it is real for  $\Lambda_\varepsilon \in (-\infty, 1)$ . Physically, imaginary  $kL$  corresponds to localized MFs at the ends of the quantum wire, and real  $kL$  indicates delocalized MFs. Those higher bands (with  $n \geq 1$ ) are associated with the excitation modes of the quantum wire, with excitation energy at least  $\Delta E$  [5].

In summary, we have

$$\frac{E(\varepsilon)}{\Delta E} = \sqrt{\Lambda_\varepsilon^2 + f_0^2(\Lambda_\varepsilon)}, \quad (\text{G6})$$

which is plotted in Fig 2a.